



Miniature free-piston homogeneous charge compression ignition engine-compressor concept—Part II: modeling HCCI combustion in small scales with detailed homogeneous gas phase chemical kinetics

H. T. Aichlmayr, D. B. Kittelson, M. R. Zachariah *

Departments of Mechanical Engineering and Chemistry, The University of Minnesota, 111 Church St. SE, Minneapolis, MN 55455, USA

Received 18 September 2001; received in revised form 7 February 2002; accepted 18 April 2002

Abstract

Operational maps for crankshaft-equipped miniature homogeneous charge compression ignition engines are established using performance estimation, detailed chemical kinetics, and diffusion models for heat transfer and radical loss. In this study, radical loss was found to be insignificant. In contrast, heat transfer was found to be increasingly significant for 10, 1, and 0.1 W engines, respectively. Also, temperature–pressure trajectories and ignition delay time maps are used to explore relationships between engine operational parameters and HCCI. Lastly, effects of engine operating conditions and design on the indicated fuel conversion efficiency are investigated.

© 2002 Published by Elsevier Science Ltd.

Keywords: Kinetic modeling; Homogeneous charge compression ignition combustion; Free-piston engine; Explosions; Micro-power generation; Microchemical

1. Introduction

This paper is the second in a two-part series that presents results of recent small-scale engine research and development activities conducted at the University of Minnesota. The first paper presented a 10 W homogeneous charge compression ignition (HCCI) engine-compressor concept and used performance estimation to explore various aspects of miniature engine design. The analysis, however, did not couple HCCI and operating parameters or account for phenomena such as enhanced heat transfer rates. Consequently, the objective of this paper is to mitigate these shortcomings by combining performance estimation with a model for small-scale HCCI combustion; resulting in plausible operational maps for miniature engines.

This paper is organized as follows. First, the HCCI model employed in this study is described. Second, models for heat transfer and radical loss in small volumes are developed. Third, relationships between engine operating

parameters and HCCI combustion are explored. Fourth, operational maps for miniature HCCI engines are established. Finally, miniature HCCI engine performance is discussed.

2. Modeling HCCI combustion

In contrast to transport-limited engine combustion modes such as spark ignition and Diesel, HCCI depends primarily upon the compression process and fuel oxidation kinetics. Therefore, matching engine operating conditions and HCCI combustion is essentially a reaction engineering problem. Generally, there are two HCCI modeling strategies: homogeneous and multi-zone. The distinction between them is whether or not gradients are assumed to exist in the combustion chamber i.e., the latter does while the former does not.

2.1. Homogeneous models

Typically, homogeneous models are developed by considering the combustion chamber to be a variable-volume batch reactor and selecting an appropriate kinetic mechanism.

* Corresponding author. Tel.: +1-612-626-9081; fax: +1-612-625-6069.

E-mail address: mrz@me.umn.edu (M. R. Zachariah).

Hence these models integrate the time-dependent energy and species conservation equations to yield temperature, pressure, and concentration histories for the charge. Najt and Foster (1983) are credited with establishing this paradigm and demonstrating that HCCI could be explained using hydrocarbon kinetics. Their efforts were followed by Lu, Gupta, Pouring, & Keating (1994) who employed Chemkin-II and a detailed hydrogen–air mechanism to investigate the role of hydrogen peroxide and radical species in HCCI. They in turn, were followed by several investigations that used HCT (Lund, 1978), detailed chemical kinetics, and bulk heat loss via the Woschni (1967) correlation (Smith, Aceves, Westbrook, & Pitz, 1997; Aceves, Smith, Westbrook, & Pitz, 1999; Flowers, Aceves, Westbrook, Smith, & Dibble, 1999; Flowers et al., 2000; Martinez-Frias, Aceves, Flowers, Smith, & Dibble, 2000). Additionally, Kelly-Zion and Dec (2000) used Chemkin-III (Kee, Rupley, & Meeks, 1996), SENKIN (Lutz, Kee, & Miller, 1988) and detailed kinetic mechanisms for *iso*-octane and *n*-heptane oxidation to determine the suitability of single- and two-stage ignition fuels for HCCI.

2.2. Multi-zone models

The strengths of homogeneous models include the ability to predict changes in ignition timing and the capability to investigate the chemistry of HCCI combustion (Lu et al., 1994; Aceves et al., 1999; Flowers et al., 1999, 2000; Kelly-Zion & Dec, 2000; Martinez-Frias et al., 2000). Unfortunately, they fail to accurately predict burn duration, peak cylinder pressure, indicated fuel conversion efficiency, and CO and hydrocarbon emissions (Christensen, Johansson, AmnJus, & Mauss, 1998; Aceves et al., 1999). Aceves et al. (1999) attribute these limitations to neglecting gradients i.e., inhomogeneity, in the combustion chamber.

Therefore to capture effects of charge inhomogeneity, Aceves et al. (2000) developed a multi-zone HCCI model. The salient features of this model include the partitioning of the combustion chamber into several homogeneous, variable-volume, batch reactors and the sequential use of KIVA (Amsden, 1993) and HCT. Initially, the distribution of mass among the zones and the initial temperature field are determined by KIVA. HCT subsequently computes temperature and species concentration histories for individual zones. Also, heat and mass transfer between zones is neglected to minimize computational requirements, but each zone features a bulk heat sink based upon the Woschni correlation. Lastly, they found excellent correspondence between model predictions and the experimental results of Christensen et al. (1998).

Aceves et al. provide many significant contributions to the understanding of HCCI. First, they give the following sequence by which HCCI combustion proceeds: (1) Chemical reactions are initiated in the center of the of the combustion chamber because it is the hottest. (2) The cen-

tral zone expands to compress adjacent zones. (3) Adjacent zones are heated by compression and chemical reactions are initiated shortly afterward. (4) Once reactions commence, these zones also expand and compress their neighbors. (5) The process repeats until the fuel in adjacent zones fails to react—which results in relatively large hydrocarbon emissions. Second, they link the ignition event to the decomposition of hydrogen peroxide and thus explain observed similarities in the behavior of various hydrocarbon fuels. Finally, Aceves et al. find that with the exception of CO and hydrocarbon emissions, the multi-zone model resolves many discrepancies between predictions and experiments. Consequently, this modeling approach has been widely adopted (Noda & Foster, 2001; Amano, Morimoto, & Kawabata, 2001; Kong, Marriott, Reitz, & Christensen, 2001; Aceves et al., 2001; Easley, Apoorva, & Lavoie, 2001; Fiveland & Assanis, 2001).

2.3. Engine cycle models

Despite their individual merits, homogeneous and multi-zone models consider only one compression–expansion cycle. Consequently, ancillary but significant processes intrinsic to the engine cycle are neglected or inappropriately modeled (Fiveland & Assanis, 2000). In contrast, an engine cycle model attempts to capture all events that occur during the cycle and may employ either the homogeneous or multi-zone approach. Examples include the free-piston engine model of Goldsborough and Van Blarigan (1999) and the four-stroke engine model of Fiveland and Assanis.

3. The miniature HCCI engine model

Although much progress has been made in understanding HCCI, the current knowledge base generally does not apply to miniature engines. For example, miniature engines are anticipated to operate between 300 Hz (18,000 RPM) and 2000 Hz (120,000 RPM). Whereas most full-size HCCI engines operate at approximately 1000 RPM. Consequently, relationships between chemical times and the engine cycle will be different. Additionally, compression ratios of 30:1 or higher, are desirable in miniature engines while compression ratios of conventional engines seldom exceed 25:1. Finally, miniature engines feature large surface-area-to-volume ratios. Hence accurate modeling of heat and mass transfer rates in these circumstances is vital and widely-used models like the Woschni (1967) correlation are inapplicable.

The objective of this work is to find combinations of operating and design conditions that are compatible with HCCI. Therefore, we concentrate our effort on the auto-ignition of the charge and defer investigations of charge inhomogeneity and regulated emissions such as NO_x, to future work. Consequently, we adopt the homogeneous modeling approach,

employ the collection of batch reactor codes that comprise SENKIN (Lutz et al., 1988), and detailed gas-phase kinetics.

3.1. Model formulation

To include effects such as heat transfer and radical loss, SENKIN is modified as follows: First, the governing equations for a non-isothermal, non-adiabatic batch reactor (closed system) are mass conservation,

$$\frac{dY_k}{dt} - v\dot{\omega}_k M_k = 0, \quad (1)$$

and the First Law of Thermodynamics for a simple compressible system viz.,

$$\frac{du}{dt} = \frac{\delta q}{dt} - \frac{\delta w}{dt}, \quad (2)$$

where Y_k and $\dot{\omega}_k$ are the mass fractions and net production rates of species k , respectively. Next, the term on the left-hand side of Eq. (2) is given by

$$\frac{du}{dt} = \sum_{k=1}^{N_s} u_k \frac{dY_k}{dt} + \sum_{k=1}^{N_s} Y_k \frac{du_k}{dt}. \quad (3)$$

Substitution of Eqs. (3) and (1) into Eq. (2) yields

$$\frac{dT}{dt} + \frac{v}{c_v} \sum_{k=1}^{N_s} u_k \dot{\omega}_k M_k + \frac{P}{c_v} \frac{dv}{dt} - \frac{1}{c_v} \frac{\delta q}{dt} = 0, \quad (4)$$

after simplification. Consequently when a mechanism of N_s species is used, Eqs. (4) and (1) comprise a set of $N_s + 1$ non-linear ordinary differential equations; integration yields $T(t)$ and $Y_k(t)$.

Note that several batch reactor models may be derived from Eq. (4). For example, discarding both work and heat transfer terms results in a fixed-volume adiabatic batch reactor model. On the other hand, if slider-crank kinematics (Heywood, 1988) are used to define $V(t)$, then a model for a crankshaft-equipped HCCI engine results ($V(t)/v$ is constant).

3.2. Heat transfer model

To model heat transfer in a miniature engine, several approaches with varying levels of complexity may be taken. To be consistent with the objectives of this study, however, the heat transfer model should be relatively simple but capture the surface-area-to-volume ratio dependence. Moreover, conduction from the charge to an isothermal wall represents a “worst case” scenario in terms of heat loss. Hence we assume conduction to be the dominant heat transfer mode.

The conduction model is developed thusly. Consider a combustion chamber of length L and bore B divided into axisymmetric regions like Fig. 1. Next, the partial differential equation

$$\frac{1}{\alpha} \frac{\partial T}{\partial t} = \nabla^2 T, \quad (5)$$

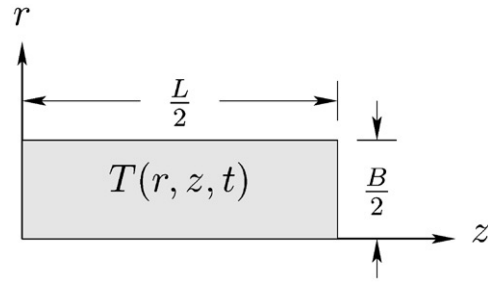


Fig. 1. Axisymmetric region used to develop the conduction model.

is solved within the domain using well-known analytical techniques and the boundary conditions

$$\begin{aligned} T(r, z, 0) &= T_0, & T(0, z, t) &\text{finite,} \\ \left. \frac{\partial T}{\partial z} \right|_{z=0} &= 0, & \left. \frac{\partial T}{\partial \phi} \right|_{\phi=0} &= 0, \\ T\left(\frac{B}{2}, z, t\right) &= T_w, & T\left(r, \frac{L}{2}, t\right) &= T_w, \end{aligned}$$

that result from assuming a uniform initial temperature, symmetry, and isothermal walls. The solution is

$$\begin{aligned} T(r, z, t) &= T_w + \frac{16(T_0 - T_w)}{B} \\ &\sum_{m=0}^{\infty} \sum_{n=1}^{\infty} \frac{(-1)^m J_0(\beta_n r) \cos(\eta_m z) \exp(-\alpha(\beta_n^2 + \eta_m^2)t)}{(2m+1)\pi\beta_n J_1(\beta_n B/2)}. \end{aligned} \quad (6)$$

Next, an average wall heat flux is derived by: (1) considering only the initial rate ($t=0$), (2) retaining only the first term of the double-infinite series i.e., $m=0$ and $n=1$, (3) computing the total wall heat flux, and (4) dividing the total wall heat flux by the surface area of the combustion chamber. This yields

$$\bar{q}'' = \frac{2k_T(T_0 - T_w)}{L} \left[\frac{0.440332\pi^2 + 5.09296(L/B)^2}{\pi + 2\pi(L/B)} \right]. \quad (7)$$

One should note that although Eq. (7) is based upon the premise that $t=0$, the expression is quasi time-dependent because L and k_T vary with time. Also, T_0 is equivalent to the bulk temperature by assumption.

Lastly, the specific heat transfer rate appearing in Eq. (4) is related to Eq. (7) by

$$\frac{\delta q}{dt} = \left(\frac{\text{surface area}}{\text{system mass}} \right) \bar{q}'', \quad (8)$$

where the surface area is given by

$$A_s = \frac{\pi B^2}{2} + \pi BL. \quad (9)$$

The relationship between heat transfer and the combustion chamber geometry may be further explored by substituting Eqs. (9), (7), and the identity $L/B = (r/(r-1))R$ into

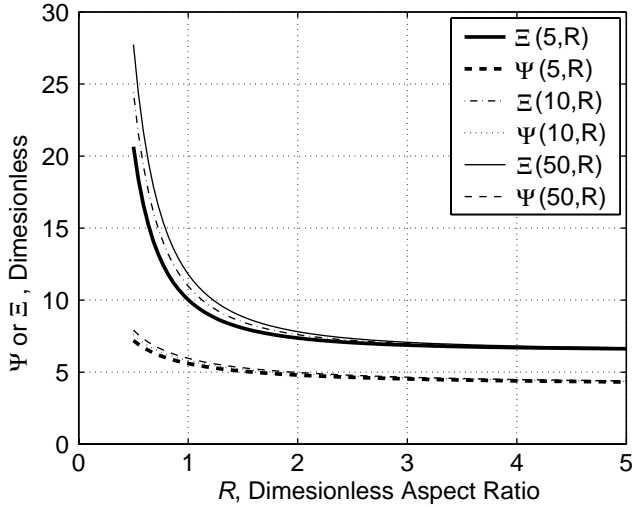


Fig. 2. Non-dimensional specific heat transfer rate (Ξ) and surface area to volume ratio function (Ψ).

Eq. (8) and rearranging. The result is a non-dimensional heat transfer rate given by

$$\begin{aligned} \Xi(r, R) &= \frac{B^2}{vk_T(T_0 - T_w)} \frac{\delta q}{dt} \\ &= \Psi(r, R) \left[\frac{2(r-1)}{rR} \right] \\ &\quad \times \left\{ \frac{0.440332\pi^2 + 5.0926(rR/(r-1))^2}{\pi + 2\pi(rR/(r-1))} \right\}. \quad (10) \end{aligned}$$

Hence the non-dimensional heat transfer rate is proportional to the non-dimensional surface-area-to-volume ratio (Ψ) and depends exclusively upon the compression ratio and the aspect ratio. For comparison, both Ξ and Ψ are plotted in Fig. 2. Evidently, large aspect ratios tend to minimize heat transfer because Ξ decreases with R . Moreover, this effect is greatest for $R < 2$ and disappears when $R > 3$. Thus $2 \leq R \leq 3$ appears to be optimal. Additionally, Fig. 2 indicates that this result is essentially independent of the compression ratio.

3.3. Radical loss model

Diffusion fluxes also increase with surface-area-to-volume ratio. Therefore assuming that radical recombination reactions on the combustion chamber walls are mass transfer-limited, we hypothesize that the frequency of these events will increase with the surface-area-to-volume ratio. Thus we model this effect by assuming the walls to be perfect radical sinks and that diffusion dominates.

Hence diffusion-limited pseudo-reactions such as



involving fictitious species (WALLH) are inserted into the kinetic mechanism. Next, the heat and mass transfer analogy

is used to obtain pseudo-heterogeneous reaction rates from Eq. (7) e.g.,

$$r''_{R1} = \frac{2\mathcal{D}_{\text{H--Air}}}{L} \left[\frac{0.440332\pi^2 + 5.09296(L/B)^2}{\pi + 2\pi(L/B)} \right] [\text{H}]. \quad (11)$$

These rates are subsequently incorporated into the kinetic mechanism via pseudo-homogeneous reaction rates (Schmidt, 1998) such as

$$r_{R1} = \left(\frac{A_s}{V(t)} \right) r''_{R1}, \quad (12)$$

where the surface area to volume ratio is given by

$$\frac{A_s}{V(t)} = \frac{2}{L} + \frac{4}{B}. \quad (13)$$

Lastly, the following is done to implement radical losses in SENKIN: (1) “Wall” species are assumed to have thermodynamic properties identical to their authentic counterparts. (2) Temperature-dependent terms of the pseudo-reaction rates are included in the kinetic mechanism while pressure and geometry-dependent parts are incorporated in the source code. (3) Transport properties of the charge are assumed identical to air and the Fuller, Schettler, and Giddings (1966) correlation is used to estimate diffusion coefficients.

4. Factors which affect HCCI in a miniature engine

To achieve HCCI, the charge must be brought by compression to a thermodynamic state such that the ignition delay time is short relative to the residence time. Therefore, in contrast to typical reaction engineering problems, the bulk temperature, chemical time, and residence time are variables. Additionally, HCCI depends strongly upon the initial conditions and the compression ratio. Hence relationships between the various parameters and HCCI are seldom obvious and we attempt to clarify them in this section.

Throughout this paper and the previous one, the fuel is assumed to be propane. Consequently, we used a mechanism developed by Westbrook (1999) and added nitrogen chemistry (Turns, 2000). The resulting mechanism is comprised of 394 species and 1909 reactions. We chose propane primarily because it has a comparatively low molecular weight and thus favorable compressive heating characteristics. Propane also exhibits essentially single-stage ignition due to mild low-temperature reactivity. Hence it offers many advantages e.g., large compression ratios may be used, for HCCI applications (Kelly-Zion & Dec, 2000).

4.1. Ignition delay time, equivalence ratio, and compressive heating

First, consider the chemical time—or in the context of HCCI—the kinetic ignition delay time. HCCI is not characterized by a fixed ignition delay time because the temperature and pressure of the charge vary during compression.

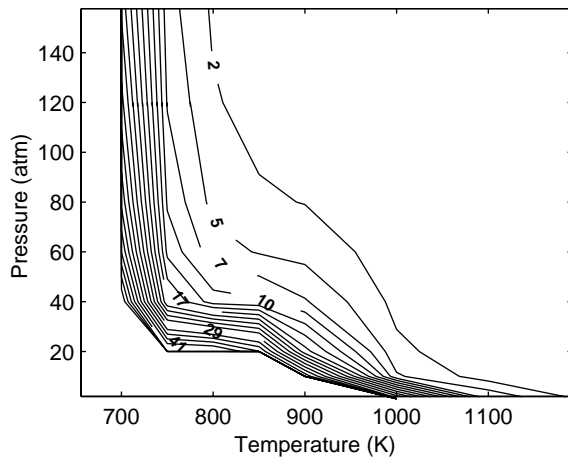


Fig. 3. Ignition delay time map for a stoichiometric mixture of propane and air. Ignition delay times are reported in milliseconds.

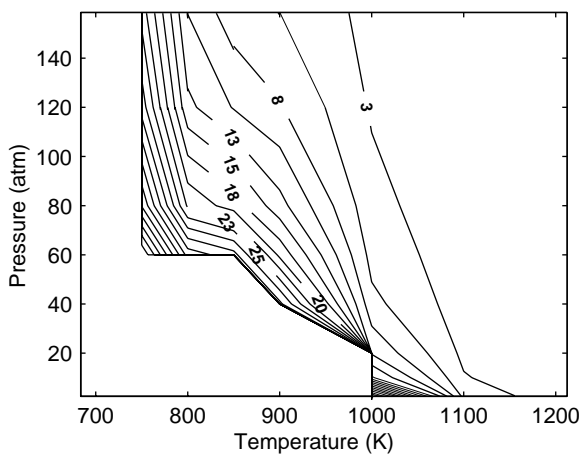


Fig. 4. Ignition delay time map for a mixture of propane and air with $\Phi = 0.2$. Ignition delay times are reported in milliseconds.

Temperature- and pressure-dependent ignition delay times however, may be readily estimated using an homogeneous, fixed-volume batch reactor model. The results of several simulations with $\Phi = 1.0$ and 0.2 are presented in Figs. 3 and 4, respectively.

According to Figs. 3 and 4, ignition delay times for a given temperature and pressure increase when the equivalence ratio is decreased. Therefore, if the time available for reaction and all other variables were fixed, one would expect a stoichiometric charge to ignite sooner than a lean charge. To test this hypothesis, an adiabatic, variable-volume batch reactor model is used to simulate engine operation with charges having equivalence ratios of 0.2 , 0.4 , 0.6 , 0.8 , and 1.0 . The results are presented in Fig. 5.

Although ignition may be defined in several ways, we assume that ignition coincides with the appearance of a sudden temperature rise i.e. a “spike”. Consequently, one may deduce from Fig. 5 that mixtures with equivalence ratios of 0.2 and 0.4 ignite while the others do not—an unexpected result.

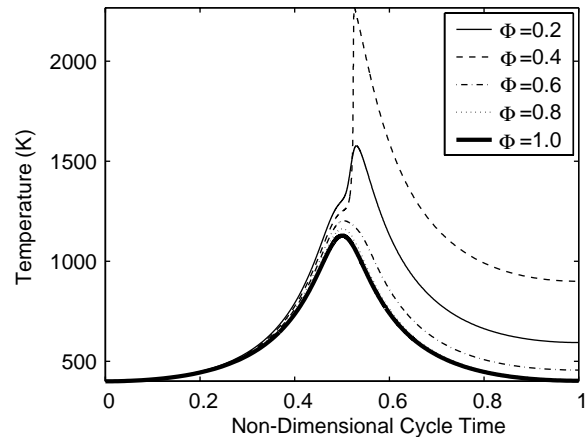


Fig. 5. Temperature profiles for an adiabatic, variable volume batch reactor model. Various equivalence ratios are considered for combustion of propane and air, $T_i = 400$ K, $P_i = 1$ atm, $N = 500$ Hz, and $r = 30$ is assumed. The non-dimensional cycle time is defined to be t/t_{Cycle} ; 0.5 corresponds to the top dead center (TDC) position in slider-crank piston motion.

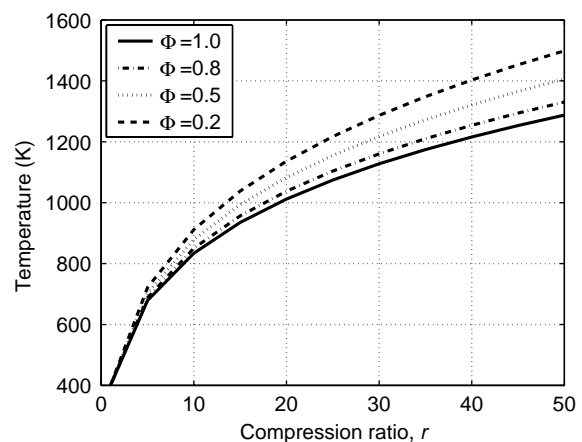


Fig. 6. Isentropic compression temperatures of propane-air mixtures obtained with EQUIL (Lutz, Rupley, Kee, Reynolds, & Meeks, 1998); $T_i = 400$ K and $P_i = 1$ atm assumed.

Of the mixtures considered in Fig. 5, one would assume from Figs. 3 and 4 that the stoichiometric mixture has the shortest ignition delay time and therefore it should ignite—yet it does not. The explanation for this counterintuitive result is that the charges do not reach the same temperature following compression. To illustrate, mixture specific heats increase with equivalence ratio. Consequently for equal compression ratios, a mixture with $\Phi = 0.4$ will have a greater temperature following compression and therefore a shorter ignition delay time, than a stoichiometric mixture (Fig. 6). Incidentally, compressive heating also causes a mixture with $\Phi = 0.2$ to ignite before $\Phi = 0.4$. One should note however, that combustion is very weak because there is little fuel to consume.

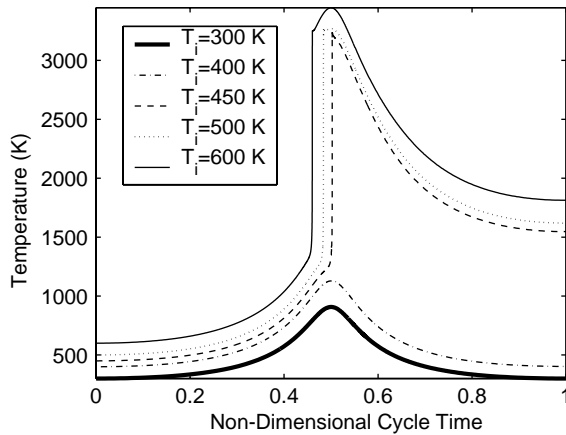


Fig. 7. Temperature profiles for an adiabatic, variable volume batch model. Various initial temperatures are considered. A stoichiometric mixture of propane and air with an initial pressure of 1 atm, compression ratio of 30:1, and engine speed of 500 Hz is assumed. The non-dimensional cycle time is defined to be t/t_{cycle} ; 0.5 corresponds to the top dead center (TDC) position of the piston.

4.2. Initial temperature

Next, the influence of the initial temperature is investigated using the adiabatic variable volume batch reactor model. Temperature–cycle time profiles for stoichiometric mixtures of propane and air are plotted in Fig. 7. For these conditions, $T_i = 450$ K is evidently the minimum initial temperature for ignition. Also note that if the temperature is increased beyond this value, ignition occurs sooner in the cycle, or it is said to be “advanced”. Consequently, this property is the basis for variable intake temperature control strategies.

Although the connection between operating parameters and fuel oxidation kinetics in HCCI is widely recognized, the nature of the relationship is difficult to discern. One approach to visualize this interaction is to consider temperature–pressure traces—or trajectories—superimposed onto ignition delay time maps e.g., Fig. 8. Note that in this representation, ignition is indicated by a trajectory which does not terminate.

An examination of the trajectories in Fig. 8 reveals that the initial temperature affects both the curvature and the termini of the trajectories. Consequently if the initial temperature were increased, the terminus of a trajectory will be translated to the right i.e., toward increasingly shorter ignition delay time contours. Therefore, the extreme initial temperature sensitivity of HCCI may be broadly attributed to the steepness of the ignition delay time surface.

4.3. Initial pressure

The influence the initial pressure is investigated in a similar manner. Initial pressures of 1, 2, 4, 5, and 8 atm are simulated and the resulting temperature–pressure trajectories are plotted in Fig. 9. Like the initial temperature, the

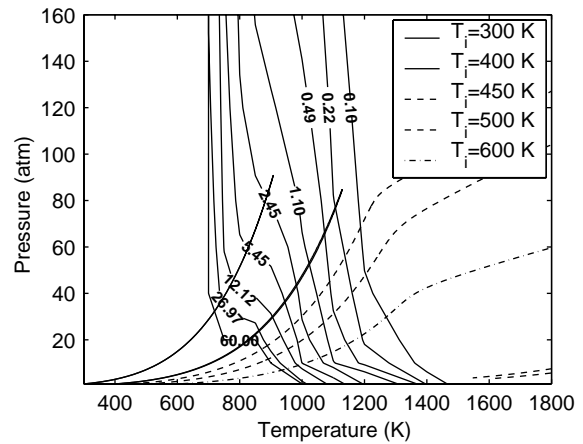


Fig. 8. Temperature–pressure trajectories superimposed on the ignition delay time map for a stoichiometric mixture of propane and air; initial temperature variations considered. Ignition delay times are reported in milliseconds.

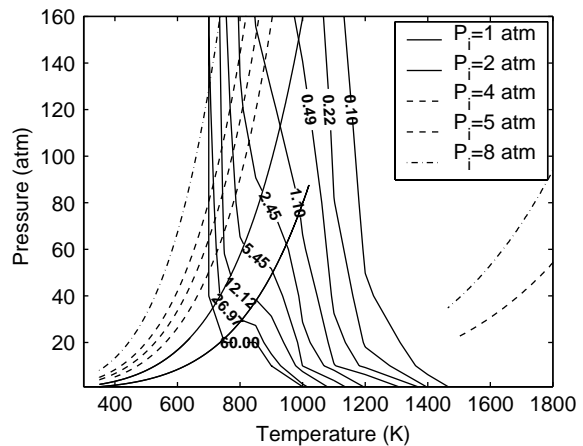


Fig. 9. Temperature–pressure paths superimposed on the ignition delay time map for a stoichiometric mixture of propane and air; initial pressure variations considered. Ignition delay times are reported in milliseconds.

initial pressure affects both the curvature and termini of the trajectories. In this case, however, the termini are translated to the left and virtually parallel to ignition delay time contours. Consequently ignition delay times do not appreciably decrease when the initial pressure is increased. Therefore, HCCI is relatively insensitive to the initial pressure. This result bodes well for supercharging because the power density can be substantially increased without affecting the ignition timing.

4.4. Compression ratio

Although fixed in a conventional engine, the compression ratio is considered here to be an operating parameter. Its influence on HCCI is also investigated using the adiabatic variable volume batch reactor model. Results of simulations with compression ratios ranging from 10 to 50 are presented in Fig. 10.

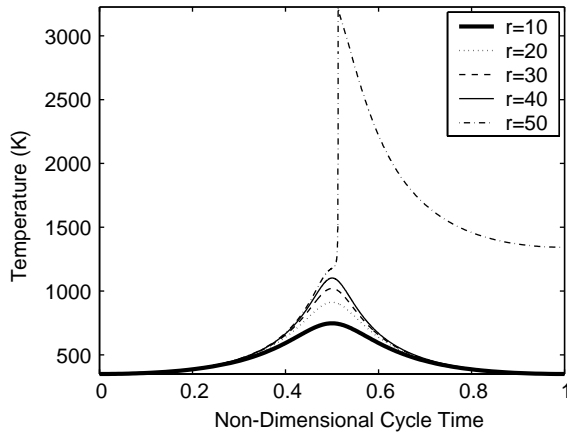


Fig. 10. Temperature profiles for an adiabatic, variable volume batch model. Various compression ratios are considered. A stoichiometric mixture of propane and air with an initial temperature and pressure of 350 K and 1 atm, respectively. The engine speed is held at 500 Hz. The non-dimensional cycle time is defined to be t/t_{cycle} ; 0.5 corresponds to the top dead center (TDC) position of the piston.

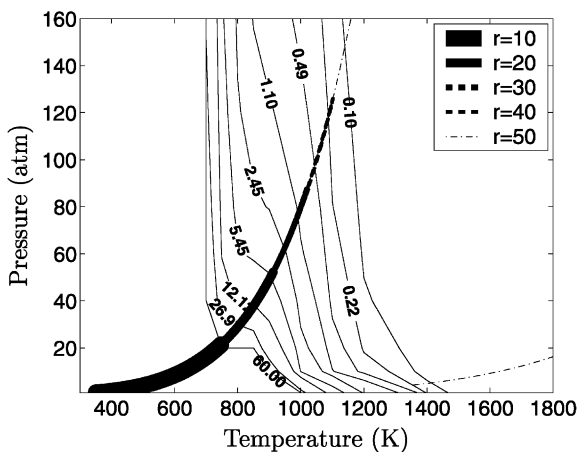


Fig. 11. Temperature–pressure paths superimposed on the ignition delay time map for a stoichiometric mixture of propane and air. Ignition delay times are reported in milliseconds.

Initially, one may conclude that varying the compression ratio is equivalent to varying the initial temperature because Fig. 10 resembles Fig. 7. This supposition, however, is invalidated upon inspection of Fig. 11. That is, in contrast to varying the initial temperature, varying the compression ratio preserves the shapes of trajectories and instead *defines* where they terminate. Consequently, *any* properly directed trajectory can be made to terminate in a region with a sufficiently short ignition delay time by increasing the compression ratio.

The preceding result is significant because it implies that ignition can be moderated in a virtually arbitrary manner if the compression ratio is a variable. To exploit this feature, however, an engine must have an infinitely variable compression ratio. Free-piston engines satisfy this requirement

and therefore offer great potential to be practical HCCI engines.

Lastly, variations in the engine speed are considered. Although ignition is not observed when a certain engine speed is exceeded, engine speed affects neither the shape nor the termini of trajectories. This result is expected because the engine speed is akin to a residence time. Therefore, it determines the ignition delay time required for ignition, but otherwise does not affect HCCI.

5. Operational maps for miniature HCCI engines

The first paper established design maps consisting of combinations of compression ratio and aspect ratio for 10 W engines. All combinations of these parameters, however, are not expected to be serviceable. Consequently, engine designs are classified according to feasibility in this section.

5.1. Radical losses

Despite the enhancement of mass transfer rates by large surface-area-to-volume ratios, radical losses are found to be negligible for a 10 W engine. In short, radical removal is much slower than radical production and ignition proceeds normally. In light of this result and the enormous computational effort required to obtain it, radical losses are henceforth neglected.

5.2. Operational maps

To systematically evaluate engine designs for compatibility with HCCI, simulations are conducted in the following way: First, a set of intake conditions i.e., an initial temperature, pressure, and equivalence ratio, are assumed. Second, pairs of aspect ratio and compression ratio (designs) are selected for evaluation. Third, engine dimensions and operating speeds are computed for the selected designs using performance estimation. Fourth, a simulation is conducted. Fifth, the engine design is designated “Ignition” or “No-Ignition”, depending upon the result of the simulation. Lastly, indicated fuel conversion efficiencies are computed. Also, both adiabatic and diathermal cases are considered.

5.2.1. Adiabatic 10 W HCCI engines—cycle and ignition delay times

An operational map for 10 W engines with $\Phi = 0.5$, $T_i = 500$ K, and $P_i = 1$ atm is presented in Fig. 12. Note that this map corresponds to the design map presented in the first paper and that values for the intake parameter ($\zeta = \rho_i/\rho_o\Phi$), are given for comparison.

Consistent with our expectations, not all engine designs in Fig. 12 are serviceable. In this case, the incompatibility of HCCI and engine designs may be attributed entirely to time effects i.e., cycle and ignition delay times, because

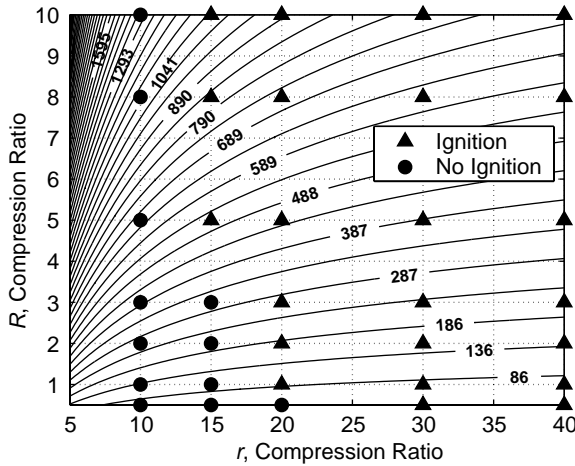


Fig. 12. Operational map for an adiabatic 10 W miniature HCCI engine operating with propane and air; $\Phi=0.5$, $T_i=500$ K, and $P_i=1$ atm ($\zeta=0.3$) is assumed. Contours indicate V_f in mm^3 .

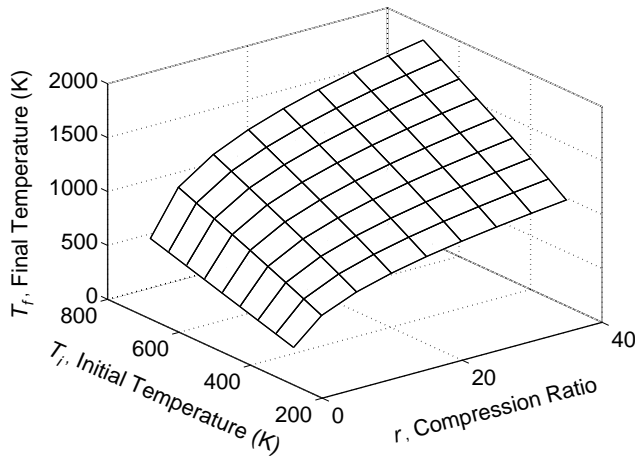


Fig. 13. The compressive heating of a stoichiometric propane-air mixture ($P_i=1$ atm).

heat transfer is excluded. First, consider the non-dimensional cycle time given by

$$\Omega(R) = \frac{\bar{U}_p}{NB} = 2R. \quad (14)$$

This parameter depends exclusively upon the aspect ratio and demonstrates that the cycle time ($1/N$), is directly proportional to R when \bar{U}_p , ζ , and r are fixed ($B = B(r, \zeta)$). Hence along the line $r = 15$, $R = 5$ corresponds to the minimum cycle time (maximum engine speed) that is compatible with HCCI under these conditions; specifically, it is 5 ms ($N = 202$ Hz). Similarly, $R = 1$ and 0.5 yield minimum cycle times of 0.95 ms ($N = 1050$ Hz) and 0.46 ms ($N = 2200$ Hz) when $r = 20$ and 30, respectively.

Next, ignition delay times decrease with compression ratio because compressive heating increases. Consequently, minimum cycle times also decrease with compression ratio. To illustrate, Figs. 13 and 14 show that compressive heating depends upon the equivalence ratio, initial conditions, and

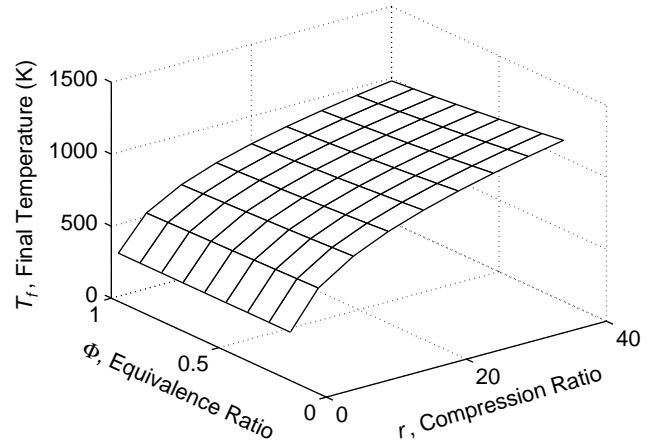


Fig. 14. The compressive heating of propane-air mixtures ($T_i = 300$ K and $P_i = 1$ atm).

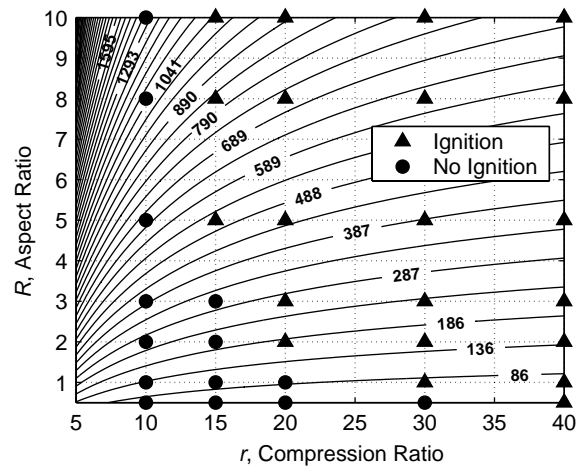


Fig. 15. Operational map for a 10 W miniature HCCI engine operating with propane and air; $\Phi = 0.5$, $T_i = 500$ K, $P_i = 1$ atm ($\zeta = 0.3$), and $T_w = 300$ K is assumed. Contours indicate V_f in mm^3 .

compression ratio, but not the aspect ratio. Hence vertical lines in Fig. 12 correspond to fixed post-compression temperatures and thus represent constant ignition delay times.

To conclude, the compatibility of an engine design with HCCI implies that the cycle time exceeds the ignition delay time. Cycle times increase with R along lines of constant compression ratio. Ignition delay times decrease with compression ratio, but are constant along lines of constant r . Designs such as $r = 15$ and $R = 5$, indicate that the cycle time slightly exceeds the ignition delay time. Therefore, any design having $r > 15$ and $R > 5$ will be compatible with HCCI; similar arguments apply to the designs $r = 20$, $R = 1$, and $r = 30$, $R = 0.5$.

5.2.2. Heat transfer

Heat transfer further constrains operational maps because it offsets compressive heating. This effect is illustrated in Fig. 15 where a wall temperature of 300 K is assumed. Note that both Figs. 12 and 15 have a similar appearance, but the

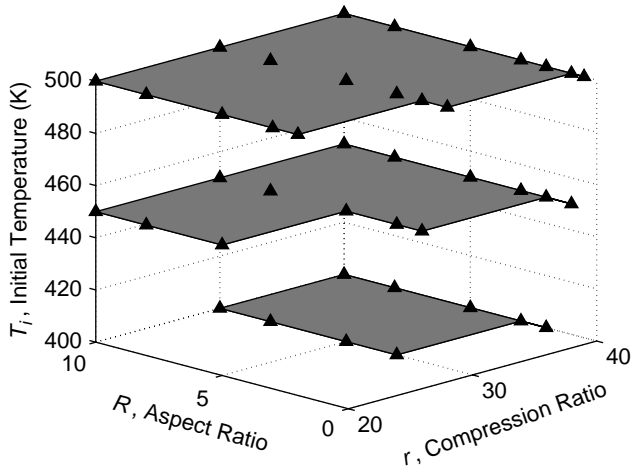


Fig. 16. Operational maps for a 10 W miniature HCCI engine operating with propane and air, $\Phi = 0.5$, $P_i = 1$ atm, and $T_w = 300$ K are assumed. The shaded areas indicate regions of operation. Also note that although cylinder volumes are not shown, they vary with the initial temperature.

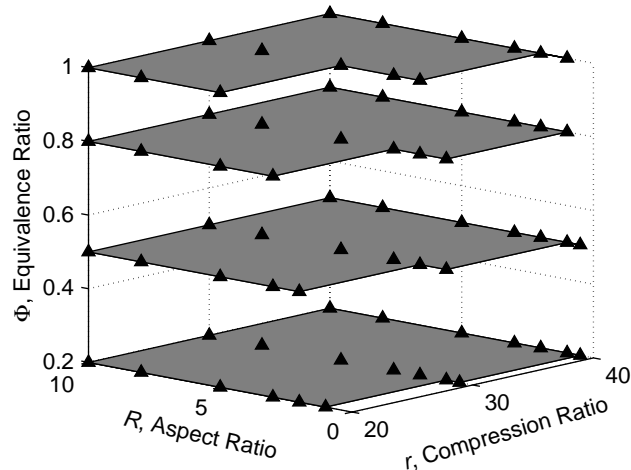


Fig. 17. Operational map for a 10 W miniature HCCI engine operating with propane and air, $T_i = 500$ K, $P_i = 1$ atm, and $T_w = 300$ K are assumed. The shaded areas indicate regions of operation. Also note that although cylinder volumes are not shown, they vary with the equivalence ratio.

designs ($r = 20, R = 1$) and ($r = 30, R = 0.5$) are excluded from the region of operation. Thus, post-compression temperatures are sufficiently reduced that ignition does not occur. Alternatively, the design ($r = 15, R = 5$) is included in the regions of operation in both Figs. 12 and 15; hence this limit is a result of time effects.

5.3. Intake conditions and operational maps

Initial conditions also affect engine operational maps. To illustrate, operational maps corresponding to initial temperatures of 400, 450, and 500 K are presented in Fig. 16. Also, equivalence ratios are held at 0.5 to facilitate comparison to Fig. 12, but one should recognize that each plane appearing in Fig. 16 represents an engine design map because

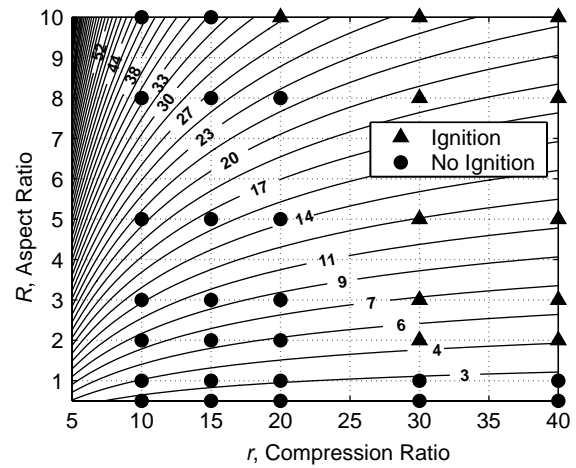


Fig. 18. Operational map for a 1 W miniature HCCI engine operating with propane and air, $\Phi = 0.5$; V_i in mm^3 , intake conditions of $T_i = 500$ K, $P_i = 1$ atm ($\zeta = 0.3$), and $T_w = 300$ K assumed. Contours indicate V_i in mm^3 .

cylinder volumes and operating speeds vary with the initial conditions. According to Fig. 16, decreasing the initial temperature contracts the boundaries of operational maps. This result is expected because the termini of temperature–pressure trajectories are translated into regions with longer ignition delay times (Fig. 8).

Next, initial temperatures are held at 500 K but equivalence ratios of 0.2, 0.5, 0.8, and 1.0 are considered. The resulting maps are plotted in Fig. 17 and the equivalence ratio is again observed to have a counterintuitive effect. That is, regions of operation are extended when the equivalence ratio is decreased. This effect is attributable to compressive heating, but one should again recognize that combustion becomes very weak when the equivalence ratio is reduced.

5.4. How small can an engine be?

Thus far, effects of heat transfer have been relatively small. According to Eq. (10), however, the specific heat transfer rate greatly increases when the engine size or aspect ratio is reduced. Therefore, one may hypothesize that heat transfer will ultimately limit the engine size.

To substantiate this hypothesis, simulations are conducted with fixed initial conditions and the power output constrained to be 1 or 0.1 W. When this is done, performance estimation demands that characteristic dimensions decrease and operating speeds increase. For example, a 10 W engine with $R = 5$ and $r = 20$ has a bore of 4.8 mm and operates at 209 Hz. A 1 W version, however, has $B = 1.5$ mm and $N = 662$ Hz while a 0.1 W version has $B = 0.5$ mm and $N = 2095$ Hz. Consequently, reducing the engine size immediately implies that ignition delay times must decrease and one would expect that greater compression ratios will be necessary.

An operational map for a 1 W engine is presented in Fig. 18. In comparison to Fig. 15, the region of operation

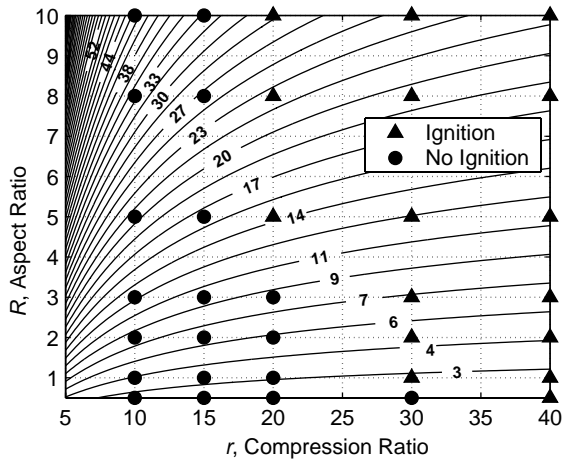


Fig. 19. Operational map for a 1 W miniature HCCI engine operating with propane and air, $\Phi=0.5$; V_i in mm^3 , intake conditions of $T_i=500$ K and $P_i=1$ atm ($\zeta=0.3$) and adiabatic is assumed. Contours indicate V_i in mm^3 .

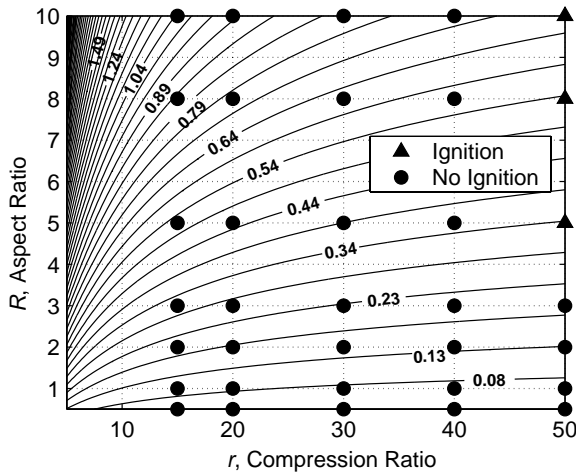


Fig. 20. Operational map for a 0.1 W miniature HCCI engine operating with propane and air, $\Phi=0.5$; V_i in mm^3 , intake conditions of $T_i=500$ K, $P_i=1$ atm ($\zeta=0.3$), and $T_w=300$ K assumed. Contours indicate V_i in mm^3 .

is significantly reduced. To determine the degree to which heat transfer is responsible, corresponding adiabatic cases are plotted in Fig. 19. Immediately, one notices that heat transfer increases the minimum aspect ratio that is compatible with HCCI. For example, when $r=20$ this threshold increases from $R \geq 5$ in Fig. 19 to $R \geq 10$ in Fig. 18. Additionally, heat transfer excludes designs with $R < 2$ regardless of any compression ratio considered.

Similarly, an operational map for a 0.1 W engine is presented in Fig. 20. Again, the region of operation is substantially reduced in comparison to Figs. 18 and 15. In fact, compression ratios less than 50 are infeasible. Examining the adiabatic cases in Fig. 21 reveals that the reduced region of operation is largely attributable to heat transfer. Hence the minimum engine size is essentially limited by heat transfer and the essence of the hypothesis is confirmed.

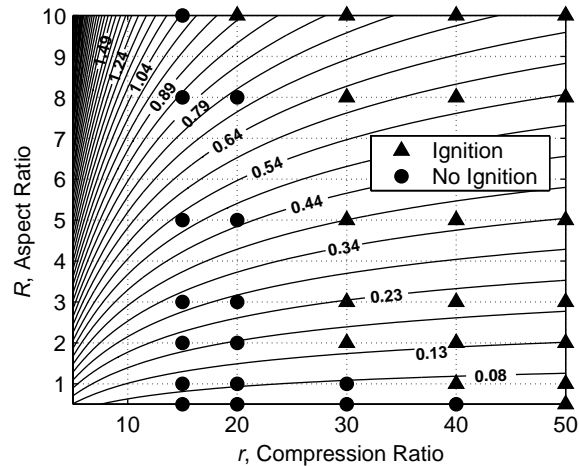


Fig. 21. Operational map for an adiabatic 0.1 W miniature HCCI engine operating with propane and air, $\Phi=0.5$; V_i in mm^3 , intake conditions of $T_i=500$ K and $P_i=1$ atm ($\zeta=0.3$). Contours indicate V_i in mm^3 .

One should note, however, that an absolute minimum engine size has not been established because effects of many parameters have not been considered.

6. Miniature HCCI engine performance

Although operational maps establish *where* in the engine design space one may operate a miniature HCCI engine, they do not provide any guidance with regard to selecting a design. To that end, power density maximization is considered here.

Recall that power density $P_d = P/V_i$, depends upon the compression ratio, aspect ratio, and initial conditions. This dependence is illustrated in Fig. 22 for $\Phi=0.5$, $T_i=500$ K, and $P_i=1$ atm ($\zeta=0.3$). Evidently, the power density is maximized for large compression ratios and small aspect ratios—a conclusion reached in the first paper. Moreover, the aspect ratio dependence is strongest.

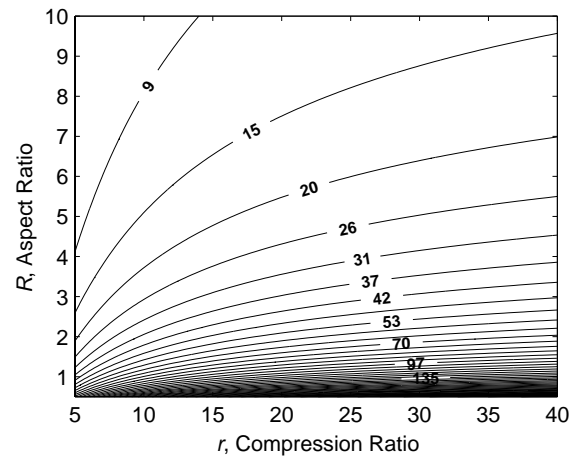


Fig. 22. Power density, P_d (W/cm^3) for a 10 W engine operating with a mixture of propane and air, $\Phi=0.5$, $T_i=500$ K and $P_i=1$ atm ($\zeta=0.3$).

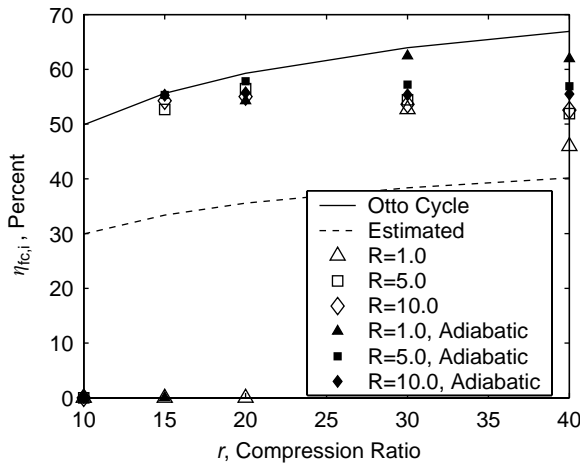


Fig. 23. The indicated fuel conversion efficiency 10 W miniature HCCI engines operating with propane and air; $\Phi = 0.5$, $T_i = 500$ K, $P_i = 1$ atm ($\zeta = 0.3$), and $T_w = 300$ K is assumed. Note that “Estimated” refers to the performance estimation result.

In the first paper, we argued that power density is maximized when the initial temperature is minimized and the initial pressure, equivalence ratio, and fuel conversion efficiency are maximized. According to Figs. 16 and 17, however, regions of operation are largest when the initial temperature is maximized and the equivalence ratio is minimized. Unfortunately, both situations decrease ζ and therefore decrease power density. Consequently engine operational space is extended at the expense of power density. Of note, this may be mitigated to some extent by supercharging, but we shall not consider it here.

Next, fuel conversion efficiencies are considered. Efficiencies corresponding to Figs. 12 and 15 are plotted in Fig. 23. Note that the efficiencies are bracketed by the Otto cycle efficiency ($\gamma = 1.3$) and the fuel conversion efficiency assumed during performance estimation (“Estimated”).

Several trends may be observed in Fig. 23. First, with the exception of cases in which the charge did not ignite ($\eta_{f,c,i} = 0$), indicated fuel conversion efficiencies exceed the estimated efficiency. Consequently, one may surmise that indicated fuel conversion efficiencies are generally under-predicted by the performance estimation process and engine designs are somewhat over-sized. Second, the Otto cycle predicts that the indicated fuel conversion efficiency increases monotonically with compression ratio. Instead, efficiencies are maximized at approximately $r = 20$ —a result shared by full-size engines. Third, heat transfer decreases efficiencies and this effect is most pronounced for small aspect ratios—both expected results. For example, heat transfer causes the case $r = 40$ and $R = 1.0$ to have the smallest observed efficiency. In contrast, the greatest efficiencies are observed when $R = 1.0$ and the engine is adiabatic. Therefore, from the perspective of maximizing the indicated fuel conversion efficiency—and thus the power density—an “optimal” engine design for this set of operating parameters would be $r = 20$ and $R = 5$.

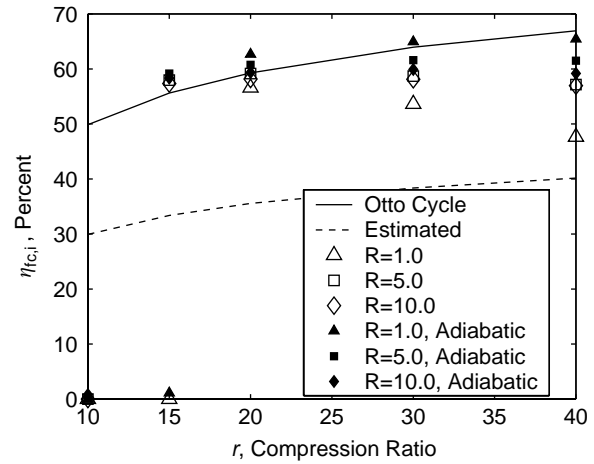


Fig. 24. The indicated fuel conversion efficiency 10 W miniature HCCI engines operating with propane and air; $\Phi = 0.2$, $T_i = 500$ K, $P_i = 1$ atm ($\zeta = 0.12$), and $T_w = 300$ K is assumed. Note that “Estimated” refers to the performance estimation result.

When the equivalence ratio is reduced to 0.2 (Fig. 24), many of the same trends may be observed. In fact, even greater efficiencies are achieved. The Otto cycle efficiency, however, is slightly exceeded—an improbable result. Subsequent comparisons between the air-standard Otto cycle and simulated P - V diagrams revealed that $\gamma = 1.35$ is a better choice when $\Phi = 0.2$. Whereas we assumed $\gamma = 1.3$ throughout.

Although the leanest cases ($\Phi = 0.2$) yield the greatest fuel conversion efficiencies, they also feature the smallest power density. Unfortunately, increased efficiencies are not able to offset this result and supercharging is likely to be a necessity should very lean mixtures be used. In contrast, if $\Phi = 1.0$ is employed to maximize power density, then efficiencies are noticeably smaller than $\Phi = 0.5$ or 0.2 (Fig. 25). Consequently a tradeoff exists between indicated fuel conversion efficiency and power density.

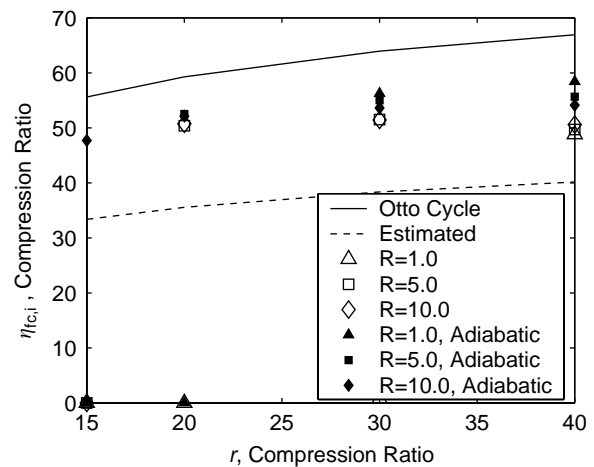


Fig. 25. The indicated fuel conversion efficiency 10 W miniature HCCI engines operating with propane and air; $\Phi = 1.0$, $T_i = 500$ K, $P_i = 1$ atm ($\zeta = 0.6$), and $T_w = 300$ K is assumed. Note that “Estimated” refers to the performance estimation result.

7. Conclusion

This paper has established operational maps for 10 W HCCI engines using performance estimation and models for HCCI combustion in small scales. HCCI combustion was modeled using detailed chemical kinetics in a variable-volume batch reactor while small-scale effects were incorporated via diffusion-based sub-models for heat and mass transfer. Operational maps were found to feature distinct boundaries between feasible and infeasible designs; a lengthy analysis followed. Additionally, size limitations for miniature HCCI engines were explored by considering power outputs of 1 and 0.1 W. Finally, the performance of miniature HCCI engines with regard to power density and indicated fuel conversion efficiency was investigated.

Significant results arising from the establishment of operational maps and the performance analysis include:

- Radical loss is negligible for a 10 W engine.
- For a 10 W engine, the boundaries of the operational zones are largely determined by the interaction of cycle time and compressive heating. Also ignition is most likely when the aspect ratio, R and the compression ratio, r are large.
- Heat transfer is greatest for small aspect ratios e.g., $R < 4$.
- A minimum HCCI engine size exists; it is determined by heat transfer.
- Increasing the initial temperature extends the boundaries of engine operation, but decreases power density.
- Decreasing the equivalence ratio also extends regions of operation and decreases the power density.
- The performance estimation method employed in the previous paper generally underpredicts the indicated fuel conversion efficiency—iteration is required.
- Heat transfer reduces indicated fuel conversion efficiencies.
- Like full-size engines, indicated fuel conversion efficiencies do not increase monotonically with compression ratio.
- The indicated fuel conversion efficiency depends upon the aspect ratio. Small aspect ratios yield the greatest efficiencies for adiabatic engines; heat transfer reverses this trend.
- Indicated fuel conversion efficiencies are greatest for lean mixtures. This effect, however, is not capable of offsetting the corresponding reduction in power density.
- In general, the extent of the engine operational space may be increased at the expense of power density.

Additionally, aspects of HCCI combustion were investigated using detailed chemical kinetics and adiabatic batch reactor models. Specifically, the significance of compressive heating was demonstrated and the interaction between engine operating parameters and chemical kinetics was explored.

The salient findings of the investigation include:

- Compressive heating is a crucial effect and yields the counterintuitive result that a lean mixture can ignite before a stoichiometric mixture.
- The initial temperature affects the curvature of temperature–pressure trajectories and translates their termini toward shorter ignition delay times. The initial pressure has a similar effect but with one key difference: The termini are translated virtually parallel to the ignition delay time contours. Due to the topography of the delay time surface, HCCI is relatively insensitive to the initial pressure and very sensitive to the initial temperature.
- The compression ratio defines the termini of temperature–pressure trajectories and does not affect their curvature. Consequently ignition may be achieved with an otherwise incompatible combination of cycle time and intake temperature by increasing the compression ratio. Little else however, is affected.
- Free-piston engines are a very promising HCCI engine concept because they feature variable compression ratios and can thus exploit the unique relationship between HCCI and compression ratio identified in this paper.

Lastly, the preceding analysis applied to crankshaft-equipped engines. Future work will abandon this assumption and couple HCCI and free-piston motion. Additionally, Aceves et al. (2000) demonstrated that charge inhomogeneity has a significant effect upon rates of pressure rise and therefore engine performance. Assuming that these effects increase with surface-area-to-volume ratios, they may ultimately constrain the combustion chamber dimensions. Consequently a multi-zonal formulation must also be considered in the future.

Notation

| | |
|-----------------------|--|
| A_s | surface area, Eq. (9), m^2 |
| B | cylinder bore, mm |
| \mathcal{D}_{H-Air} | binary diffusion coefficient, Eq. (11), cm^2/s |
| J_0 | zero-order Bessel function of the first kind, Eq. (6) |
| J_1 | first-order Bessel function of the first kind, Eq. (6) |
| k | subscript for a species, Eq. (1), unitless |
| k_T | thermal conductivity, Eq. (7), W/mK |
| L | combustion chamber length, mm |
| m | summation index, Eq. (6), unitless |
| M_k | molecular weight of species k , Eq. (1), g/mol |
| n | summation index, Eq. (6), unitless |
| N | engine speed, Eq. (14), Hz |
| N_s | total number of species, Eq. (3), unitless |
| P_d | power density, $(P/V_t = 4P/\pi RB^3)$, W/cm^3 |
| q | specific heat transfer, Eq. (2), kJ/kg |
| \bar{q}'' | average heat flux, Eq. (7), W/m^2 |

| | |
|-------------|--|
| r | radial coordinate or compression ratio |
| r_{R1} | pseudo-homogeneous reaction rate, Eq. (12), mol/cm ³ s |
| r''_{R1} | heterogeneous reaction rate, Eq. (11), mol/cm ² s |
| R | stroke to bore aspect ratio ($\frac{S}{B}$), Eq. (10), dimensionless |
| S | piston stroke, m |
| t | time, Eq. (1), s |
| T | temperature, Eq. (4), K |
| T_w | uniform wall temperature, Eq. (5), K |
| T_0 | uniform initial temperature, Eq. (5), K |
| u | specific internal energy, Eq. (2), kJ/kg |
| u_k | internal energy of species k , Eq. (3), kJ/kg |
| \bar{U}_p | mean piston speed, Eq. (14), m/s |
| v | specific volume, Eq. (1), m ³ /kg |
| $V(t)$ | time-dependent combustion chamber volume m ³ |
| V_t | total cylinder volume ($\pi B^2 L/4$), mm ³ |
| w | work per unit mass, Eq. (2), kJ/kg |
| Y_k | mass fraction of species k , Eq. (1), unitless |
| z | axial coordinate |

Greek letters

| | |
|------------------|--|
| α | thermal diffusivity, Eq. (5), m ² /s |
| β_n | eigenvalue defined by $J_0(\beta_n B/2) = 0$, Eq. (6) |
| γ | mixture specific heat ratio, dimensionless |
| ζ | intake parameter ($(\rho_i/\rho_o)\Phi$), dimensionless |
| $\eta_{f,c,i}$ | fuel conversion efficiency of the engine cycle, dimensionless |
| η_m | eigenvalue given by $(2m + 1)\pi/L$, Eq. (6) |
| Ξ | non-dimensional specific heat transfer rate ($\Xi(r, R) = B^2/vk_T(T_0 - T_w)\delta q/dt$), Eq. (10) |
| ρ_i | density of air at the intake, kg/m ³ |
| ρ_o | density of air at 300 K and 1 atm, kg/m ³ |
| Ψ | non-dimensional surface-area-to-volume ratio ($\Psi(r, R) = BA_s/V$), Eq. (10) |
| $\dot{\omega}_k$ | molar production rate of species k , Eq. (1), mol/cm ³ s |
| Ω | non-dimensional engine speed ($\Omega(R) = \bar{U}_p/NB = 2R$), Eq. (14) |

Acknowledgements

This project was sponsored by Honeywell International under DARPA contract no. F30602-99-C-0200. The authors would also like to acknowledge the support of the Minnesota Supercomputing Institute.

References

Aceves, S. M., Flowers, D. L., Martinez-Frias, J., Smith, J. R., Westbrook, Charles, K., Pitz, W. J., Dibble, R., Wright, J. F., Akinyemi, W. C.,

& Hessel, R. P. (2001). A sequential fluid-mechanic chemical-kinetic model of propane HCCI combustion. In: J. Rey Agama & J. D. Hiltner (Eds.), *Homogeneous charge compression ignition (HCCI) combustion*, SP-1623 (pp. 51–61). Warrendale, PA: Society of Automotive Engineers.

Aceves, S. M., Flowers, D. L., Westbrook, C. K., Smith, J. R., Pitz, W., Dibble, R., Christensen, M., & Johansson, B. (2000). *A multi-zone model for prediction of HCCI combustion and emissions*. SAE Technical Paper 2000-01-0327.

Aceves, S. M., Smith, J. R., Westbrook, C. K., & Pitz, W. J. (1999). Compression ratio effect on methane HCCI combustion. *Journal of Engineering for Gas Turbines and Power*, 121(3), 569–574.

Amano, T., Morimoto, S., & Kawabata, Y. (2001). Modeling the effect of air/fuel ratio and temperature distribution on HCCI engines. In: J. Rey Agama & J. D. Hiltner (Eds.), *Homogeneous charge compression ignition (HCCI) combustion*, SP-1623 (pp. 23–29). Warrendale, PA: Society of Automotive Engineers.

Amsden, A. A. (1993). *KIVA-3: A KIVA program with block-structured mesh for complex geometries*. Report LA-12503-MS, Los Alamos National Laboratory, Los Alamos, NM.

Christensen, M., Johansson, B., AmnJus, P., & Mauss, F. (1998). *Supercharged homogenous charge compression ignition*. SAE Technical Paper 980787.

Easley, W. L., Apoorva, A., & Lavoie, G. A., 2001. Modeling HCCI combustion and emissions using detailed chemistry. In: J. Rey Agama & J. D. Hiltner (Eds.), *Homogeneous charge compression ignition (HCCI) combustion*, SP-1623 (pp. 79–95). Warrendale, PA: Society of Automotive Engineers.

Fiveland, S. B., & Assanis, D. N. (2000). *A four-stroke homogeneous charge compression ignition engine simulation for combustion and performance studies*. SAE Technical Paper 2000-01-0332.

Fiveland, S. B., & Assanis, D. N. (2001). Development of a two-zone HCCI combustion model accounting for boundary layer effects. In: J. Rey Agama & J. D. Hiltner (Eds.), *Homogeneous charge compression ignition (HCCI) combustion*, SP-1623 (pp. 63–77). Warrendale, PA: Society of Automotive Engineers.

Flowers, D., Aceves, S., Smith, R., Torres, J., Girard, J., & Dibble, R. (2000). *HCCI in a CFR engine: Experiments and detailed kinetic modeling*. SAE Technical Paper 2000-01-0328.

Flowers, D., Aceves, S., Westbrook, C. K., Smith, J. R., & Dibble, R. (1999). Sensitivity of natural gas HCCI combustion to fuel and operating parameters using detailed kinetic modeling. In: S.M. Aceves, S.Garimella, & R. Peterson (Eds.), *Proceedings of the American society of mechanical engineers advanced energy systems division*, AES-Vol. 39 (pp. 465–474). New York, NY: American Society of Mechanical Engineers.

Fuller, E. N., Schettler, P. D., & Giddings, J. C. (1966). A new method for prediction of binary gas-phase diffusion coefficients. *Industrial and Engineering Chemistry*, 58(5), 19–27.

Goldsborough, S. S., & Van Blarigan, P. (1999). *A numerical study of a free piston IC engine operating on homogeneous charge compression ignition combustion*. SAE Technical Paper 990619.

Heywood, J. B. (1988). *Internal combustion engine fundamentals*. New York: McGraw-Hill.

Kee, R. J., Rupley, F. M., & Meeks, E. (1996). *Chemkin-III: A Fortran chemical kinetics package for the analysis of gas-phase chemical and plasma kinetics*. Sandia Report SAND96-8216, Sandia National Laboratory.

Kelly-Zion, P. L., & Dec, J. E. (2000). A computational study of the effect of fuel-type on ignition time in HCCI engines. In *Twenty-eighth symposium (international) on combustion*. Pittsburgh, PA: The Combustion Institute.

Kong, S.-C., Marriott, C. D., Reitz, R. D., & Christensen, M. (2001). Modeling and experiments of HCCI engine combustion using detailed chemical kinetics and multidimensional CFD. In: J. Rey Agama & J. D. Hiltner (Eds.), *Homogeneous charge compression ignition*

- (HCCI) combustion, SP-1623 (pp. 39–50). Warrendale, PA: Society of Automotive Engineers.
- Lu, J., Gupta, A. K., Pouring, A. A., & Keating, E. L. (1994). *A preliminary study of chemically enhanced autoignition in an internal combustion engine*. SAE Technical Paper 940758.
- Lund, C. M. (1978). *HCT—a general computer program for calculating time-dependent phenomena involving one-dimensional hydrodynamics, transport, and detailed chemical kinetics*. Report UCRL-52504, Lawrence Livermore National Laboratory, Livermore, CA.
- Lutz, A. E., Kee, R. J., & Miller, J. A. (1988). *Senkin: A Fortran program for predicting homogeneous gas phase chemical kinetics with sensitivity analysis*. Sandia Report SAND87-8248, Sandia National Laboratory.
- Lutz, A. E., Rupley, F. M., Kee, R. J., Reynolds, W. C., & Meeks, E. (1998). *EQUIL: A CHEMKIN implementation of STANJAN for computing chemical equilibria*. Reaction Design Inc., 6500 Dublin Boulevard, Dublin, CA 94568, USA. Manual authorised by E. Meets.
- Martinez-Frias, J., Aceves, S. M., Flowers, D., Smith, J. R., & Dibble, R. (2000). Exhaust energy recovery for control of a homogeneous charge compression ignition engine. In: S. Garimella, M. von Spakovsky, & S. Somasundaram (Eds.), *Proceedings of the American society of mechanical engineers advanced energy systems division*, AES-Vol. 40 (pp. 349–356). New York, NY: American Society of Mechanical Engineers.
- Najt, P. M., & Foster, D. E. (1983). *Compression-ignited homogeneous charge combustion*. SAE Technical Paper 830264.
- Noda, T., & Foster, D. E., 2001. A numerical study to control combustion duration of hydrogen-fueled HCCI by using multi-zone chemical kinetics simulation. In: J. Rey Agama & J. D. Hiltner (Eds.), *Homogeneous charge compression ignition (HCCI) combustion*, SP-1623 (pp. 9–14). Warrendale, PA: Society of Automotive Engineers.
- Schmidt, L. D. (1998). *The engineering of chemical reactions*. New York: Oxford University Press.
- Smith, J. R., Aceves, S. M., Westbrook, C., & Pitz, W. (1997). Modeling of homogeneous charge compression ignition (HCCI) of methane. In: T. Uzkan (Ed.), *Predictive engine design, validation and experiment*, ICE-Vol. 29-3, *Engine combustion performance and emissions*, Vol. 3, *Proceedings of the 19th annual fall technical conference of the ASME internal combustion engine division*, Madison, WI, 9/28–10/1 (pp. 85–90). New York, NY: American Society of Mechanical Engineers.
- Turns, S. R. (2000). *An introduction to combustion concepts and applications* (2nd ed.). Boston: Mc-Graw Hill.
- Westbrook, C. K. (1999). Personal communication.
- Woschni, G. (1967). *A universally applicable equation for the instantaneous heat transfer coefficient in the internal combustion engine*. SAE Technical Paper 670931.